JOURNAL OF CATALYSIS **163,** 465–475 (1996)
ARTICLE NO. 0348

Effect of Flow Rate on the Partial Oxidation of Methane and Ethane[1]

P. M. Witt and L. D. Schmidt

Department of Chemical Engineering and Materials Science, University of Minnesota, Minneapolis, Minnesota 55455-0132

Received April 10, 1996; revised June 20, 1996; accepted June 21, 1996

The partial oxidation of CH_4 over rhodium coated monoliths and C_2H_6 over platinum coated monoliths was examined in the fuel rich regime at space velocities up to 4×10^6 h^{-1} (~200 μs), a variation by a factor of 50. For CH_4, the conversion drops from 90% at 5×10^4 h^{-1} to 20% at 1×10^6 h^{-1}, while for C_2H_6, the conversion and the selectivity to C_2H_4 remain nearly constant up to 4×10^6 h^{-1}. For CH_4, the O_2 conversion drops below 100% at 5×10^5 h^{-1} but remains complete in the oxidation of C_2H_6. As the space velocity increases in CH_4 oxidation, the temperature of the leading edge of the monolith decreases from 900°C at 1×10^5 h^{-1} to 60°C at 1×10^6 h^{-1}. The cool region of the monolith promotes the formation of total oxidation and also the production of CH_3 radicals which lead to the formation of C_2 coupling products in the gas phase. A maximum in coupling selectivity of 10% is observed at 5.5×10^5 h^{-1} and 270°C preheat.

1. INTRODUCTION

There has been a growing interest in the direct conversion of natural gas into more valuable products. Recent research has shown that CH_4, the largest component of natural gas, can be converted to synthesis gas by passing it premixed with oxygen over a Rh coated ceramic monolith at contact times of several milliseconds (1–3)

$$CH_4 + 1/2\ O_2 \rightarrow CO + 2H_2. \quad [1]$$

This process runs autothermally and achieves >90% selectivity to syngas at >90% conversion of CH_4 and 100% conversion of O_2. It has also been shown that at these short contact times steam reforming

$$CH_4 + H_2O \rightarrow CO + 3H_2 \quad [2]$$

and water gas shift

$$CO + H_2O \rightarrow CO_2 + H_2 \quad [3]$$

reactions do not strongly affect the product distribution (2).

The direct conversion of CH_4 to syngas has also been studied at longer contact times (~200 ms); in a fluidized bed reactor (4) using Rh supported on 100 μm α-Al_2O_3 beads to achieve selectivities and conversions similar to the Rh coated monolith. The first step in the surface mechanism for CH_4 conversion to syngas over Rh is postulated to be the pyrolysis of CH_4 on the surface

$$CH_4 \rightarrow C_s + 4H_s \quad [4]$$

where s indicates surface species (5). The surface C and H then react with absorbed O to form CO, CO_2 and H_2O, while H_s dimerizes to form H_2. This model predicts the reaction products extremely well, although, the mechanism does not include routes to higher carbon number chemicals which typically are observed with selectivities much less than 1% (2, 6).

Under similar experimental conditions, the partial oxidation of C_2H_6 to ethylene

$$C_2H_6 + 1/2\ O_2 \rightarrow C_2H_4 + H_2O \quad [5]$$

over Pt coated α-Al_2O_3 monoliths gives selectivities to ethylene of ~65% at C_2H_6 conversions of 80% (7). This reaction runs autothermally at contact times of ~5 ms. Ethane is postulated to adsorb on the Pt surface via a single H abstraction by absorbed oxygen,

$$C_2H_6 + O_s \rightarrow C_2H_{5s} + OH_s, \quad [6]$$

forming absorbed ethyl and hydroxyl species. The hydroxyl species then abstracts a second hydrogen through a β-elimination mechanism to form C_2H_4 and H_2O in the gas phase (32).

Previous research on the production of syngas and ethylene from CH_4 and C_2H_6 respectively have emphasized the importance of short contact times to obtain adiabatic operation and non equilibrium product distributions. However, no systematic studies with variable contact time have been reported. This research represents an attempt to react CH_4 to synthesis gas and C_2H_6 to ethylene at contact times on the order of 100 μs. Reactions at these contact times may give insight into the primary reaction steps governing these processes. Further, the economics of these processes depend strongly on the residence time which determines the size of the reactor required for a given production rate.

[1] This research was partially supported by NSF under Grant CTS-9311295-02 and DOE under Grant DE-FG02-88ER13878.

0021-9517/96 $18.00

2. EXPERIMENTAL

Gases flowed at high velocities through a foam monolith coated with noble metal as described previously (1, 4, 6, 7). After ignition, the overall exothermicity of the reaction maintains the monolith at high enough temperatures to sustain adiabatic operation. By varying the space velocity, feed composition, and preheat, different aspects of the reaction system can be investigated such as the production capability of a single monolith and the major reaction steps on noble metal coated monoliths.

Apparatus

The apparatus consisted of quartz reactor tubes 40 cm long with 18, 11, and 5 mm inside diameters. A cylindrical α-Al_2O_3 (92% α-Al_2O_3, 8% SiO_2) foam monolith 1 cm long and coated with noble metal (Rh for syngas and Pt for olefins) was used as the catalyst. The monolith was wrapped with a thin layer of silica–alumina insulation to prevent gases from bypassing the catalyst. Inert extruded cordierite monoliths before and after the catalyst minimized radiant heat losses in the axial direction. Adiabatic operation was insured by wrapping the quartz tube with 0.5 in. layer of insulation.

Gas flow rates were controlled by mass flow controllers to an accuracy of 0.1 SLPM. The gases were premixed prior to entering the reaction zone. Since N_2 is inert in this system, it was added to the feed stream as a GC standard to account for the volume expansion caused by reaction. The product lines were heated with heating tape to prevent water condensation. Reaction products were analyzed by an on-line GC and incinerated. The GC was an HP 5890 with a 5A mole sieve to separate O_2, N_2, CH_4 and CO and a Haysep D column to separate all other species. Mole balances generally closed within 3%. CO and CO_2 were the only oxygenated carbon products detected in both the CH_4 and C_2H_6 oxidation systems except for small amounts of acetaldehyde (<0.1%) in C_2H_6 oxidation. Total gas flow rates ranged from 2 to 25 SLPM.

The temperature of the front face of the monolith was measured with a bare chromel/alumel thermocouple located between the upstream radiation shield and the catalytic monolith. The back face temperature was monitored with a bare Pt/Pt-13% Rh thermocouple located between the catalytic monolith and the downstream radiation shield. The measured exit temperatures were always within 100°C of the calculated adiabatic flame temperature based on the product compositions. The accuracy of the entrance temperature measurement depended strongly on consistent placement of the thermocouple junction, and values reported could be low by as much as 100°C. The overall pressure of the system was maintained at 1.4 atm to overcome pressure drop restrictions (<0.2 atm) between the reactor and GC.

Catalyst Preparation

The catalysts were prepared by impregnating a monolith with saturated solutions of $RhCl_3$ in acetone for Rh and H_2PtCl_6 in water for Pt as described previously (2, 6, 7). After the monolith was saturated and dried in air, it was calcined in oxygen at 600°C for an hour and reduced in 10% H_2/Ar at 600°C for 4 h. This procedure resulted in loadings of approximately 5 wt%. The α-Al_2O_3 monoliths contain macropores (45 ppi) with a void fraction of 0.8, and are not microporous, having a surface area of only 100 cm^2/g.

Previously, we have reported analysis detailing the microstructure and surface composition of similar catalysts (8). Fresh catalysts were uniformly covered with 1 μm diameter crystallites of noble metal. Over many hours of operation at 1000°C, negligible metal is lost from both Rh and Pt coated foam monoliths. The vapor pressures of Rh (2.5×10^{-7} atm at 1730°C) and Pt (1.3×10^{-12} atm at 1230°C) are low (36), and metal loss is only a problem with more volatile metals such as Ni and for Pt in excess oxygen.

Experiment

The fuel to oxygen ratios were based on optimal product selectivities at a gas hourly space velocity (GHSV) of $1 \times 10^5\ h^{-1}$, as reported elsewhere. The optimal production of syngas from CH_4 occurs at CH_4/O_2 ratio of ~1.8 (1, 4), while the optimal production of ethylene is at C_2H_6/O_2 of ~1.7 (2, 7). In most experiments we did not consider the variation of composition from these values.

To initiate the reaction for C_2H_6, the fuel to oxygen ratio in the feed mixture was lowered to a value slightly above stoichiometric for syngas production and the catalyst was then preheated with a Bunsen burner to roughly 200–400°C to ignite the catalyst. The Bunsen burner was then removed and no further heat input was required to maintain reaction. Finally, the fuel of oxygen ratio was returned to the desired experimental conditions for operation.

Ammonia was used to initiate the CH_4 reaction (6). After ignition, the ammonia was replaced by CH_4 and the fuel to oxygen ratio was altered to operating conditions.

Carbon and hydrogen atom selectivities are determined from molar flow rates as described previously (8).

Contact Time

Previously we have reported results as a function of contact time, τ, based on reaction conditions. This is possible because at 1 ms the temperature is constant to within ~100°C over the length of the catalytic monolith (9) so that $\tau = l/u$ can be easily calculated from the flow rate. However, as the flow rate increases, the temperature profile changes because the front surface cools, and to determine the contact time accurately, the axial temperature profile would

have to be integrated across the monolith. However, since the exact temperature profile is unknown and the conversion varies, we use space velocity here.

Space velocity SV is defined as the ratio of volumetric flow rate v_0 to the reactor void volume V at standard temperature and pressure of 25°C and 1 atm,

$$\mathrm{SV} = v_0/V. \qquad [7]$$

Space velocity is the reciprocal of the residence time if gases remained at 25°C and 1 atm.

In the figures we indicate minimum and maximum τ for these space velocities. At low space velocity, τ is accurate; but at high SV, τ is an approximation.

Oxygen Breakthrough

An important feature of our previous monolith experiments was oxygen conversion in excess of 99% (4, 6, 10, 11). At higher space velocity, we find that the oxygen conversion decreases substantially. This can results in the ignition of the downstream Pt/Pt-10% Rh thermocouple and possible homogeneous reaction. This may affect the exit temperature measurement when oxygen breakthrough is significant. However, we still indicate thermocouple temperature measurements even though they may be less accurate under these conditions.

Standing flames. As the space velocity is pushed upwards of 1×10^6 h^{-1}, the system becomes more sensitive to moderate perturbations in flow rate. When the flow of one species is increased abruptly at high space velocities, a standing blue flame was sometimes visible downstream of the catalyst. This flame is stable and only extinguishes by decreasing the flow rate considerably *beyond* the previous stable nonflame condition. This indicates that the monolith can operate in two modes: one as catalytic partial oxidation and the other where the extinguished catalyst acts as a flame holder.

Temperature variation. The hot section of the monolith moves into the catalyst as the space velocity changes. At very low space velocities the front edge of the monolith glows brighter than the back edge. As the space velocity increases to about 1×10^5 h^{-1}, the entire monolith glows equally bright. Beyond 1×10^5 h^{-1}, the front edge of the monolith become dark, while the back edge glows extremely bright (even hotter than when the temperature is uniform). At all flow rates, no intermediate position within the monolith glowed brighter than either end.

3. ETHANE OXIDATION

Figure 1 shows the effect of increasing the space velocity from 1×10^5 h^{-1} ($\tau \sim 10$ ms) to 4×10^6 h^{-1} ($\tau \sim 200$ μs)

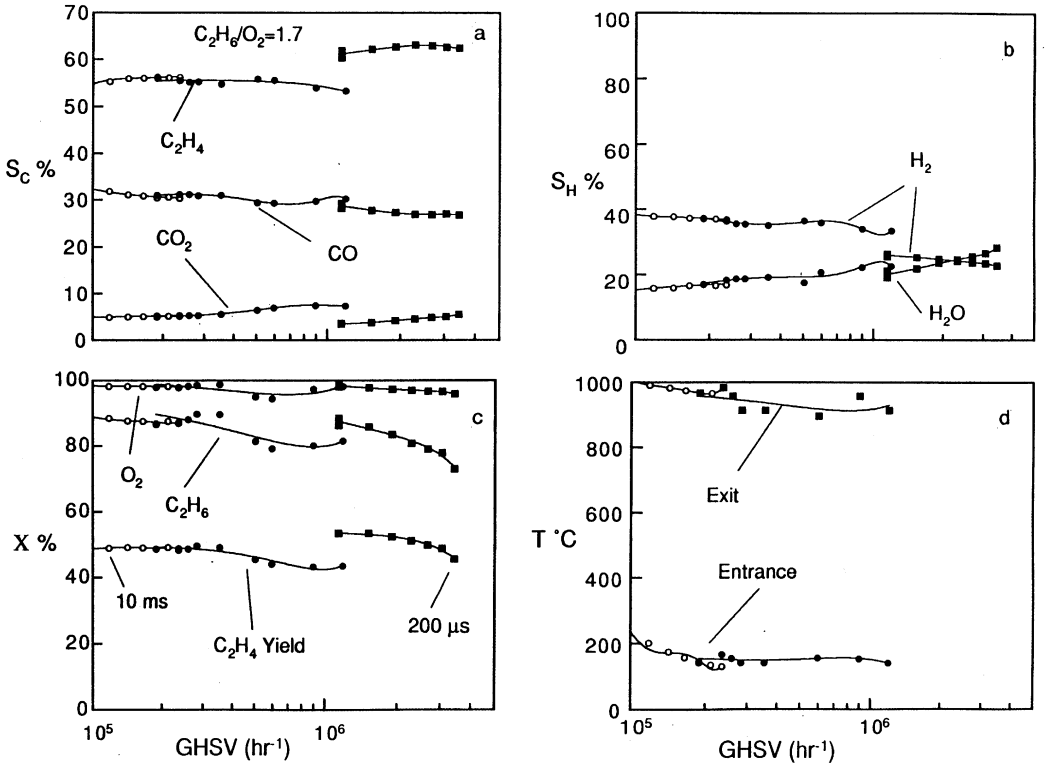

FIG. 1. Ethane partial oxidation. Carbon atom (a) and hydrogen atom (b) selectivities, and CH_4, O_2 conversion (c) for the partial oxidation of C_2H_6 over Pt supported α-Al_2O_3 foam monoliths. Space velocities are calculated at standard temperature and pressure. $C_2H_6/O_2 = 1.7$, 20% N_2. Open circles 18 mm, filled circles 11 mm, filled squares 5 mm.

using 18 mm (open circles), 11 mm (closed circles), and 5 mm (squares) diameter monoliths. The carbon atom selectivity to C_2H_4, panel (a), is nearly independent of space velocity up to 4×10^6 h^{-1}. The selectivity to C_2H_4 appears to jump to ~62% and remain constant from 1×10^6 to 4×10^6 h^{-1}. This jump coincides with a switch to 5 mm diameter catalyst, and we believe the geometrical differences between the 5 and the 11 mm monolith probably caused this change. This break is also evident in the other three panels of Fig. 1. We repeated these experiments on several catalysts, and the break between the 5 and 11 mm catalysts was consistent as shown. The break between the 11 mm and 5 mm diameter monoliths is small; however, a more significant discontinuity is seen in the CH_4 system, as we will show later.

The hydrogen atom selectivity, panel (b), is more sensitive to space velocity than the carbon atom selectivity panel (c), which remains nearly constant. The selectivity to H_2 decreases from 38% at 1×10^5 h^{-1} to 20% at 4×10^6 h^{-1}. A jump in C_2H_6 conversion and C_2H_4 yield is observed when we switched to the 5 mm diameter monolith, although, they both begin to decrease immediately. The C_2H_6 conversion drops from 90% to ~75% while the C_2H_4 yield decreases from 55% to 50%. The O_2 conversion remains above 97% up to the highest space velocities.

An important result is even at extremely high flow rates the conversions of C_2H_6 and O_2 remain high, panel (c). The high conversion combined with a high selectivity to C_2H_4 results in C_2H_4 yield of 48%. This yield at 4×10^6 h^{-1} means that we would produce 200 lbs/day of ethylene in a single 1.8 cm diameter, 1 cm long Pt coatedmonolith and ~130 tons/day in a single 1 ft diameter, 1 cm long monolith operated under identical conditions.

The exit temperature of the monolith, panel (d), decreased from 1000°C at 10^5 h^{-1} to 900°C at ~10^6 h^{-1}, while the entrance temperature only decreased approximately 50°C. The exit temperature always remained within 100°C of the calculated adiabatic temperature.

4. METHANE OXIDATION

Space velocity. Figure 2 shows data over 5.5 wt% Rh coated α-Al_2O_3 monoliths. Panels (a), (b), and (c) show how the carbon atom selectivity, hydrogen atom selectivity, and the conversion of CH_4 change with variation in space velocity by a factor of 50 while panel (d) shows how the temperatures of the front and back faces of the catalytic monolith vary with space velocity. The selectivity to all products

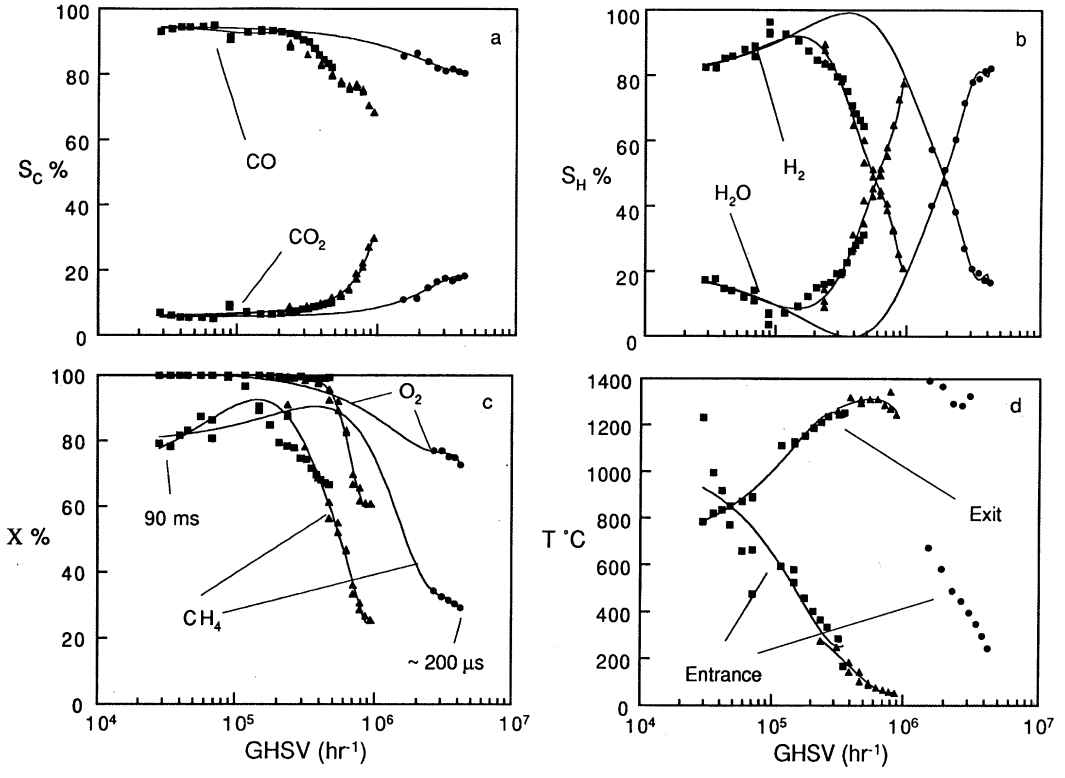

FIG. 2. Methane partial oxidation. Carbon atom (a) and hydrogen atom (b) selectivities, O_2 and CH_4 conversion (c) and entrance and exit temperatures (d) for the partial oxidation of methane over Rh supported foam monoliths. The curves connect data from 18 mm with 11 mm and 5 mm monoliths. Space velocities are calculated at standard temperature and pressure. 20% N_2, $CH_4/O_2 = 1.8$. Filled squares 18 mm, filled triangles 11 mm, filled circles 5 mm.

at 1×10^5 h^{-1} are in good agreement with previously published results (6).

Close inspection of Fig. 2 reveals differences between the different diameter tubes and monoliths. The data collected from the 18 mm and 11 mm tubes cover space velocities from 5×10^4 to 1×10^6 h^{-1}. Data points overlap well for the 18 and 11 mm data. However, data does not overlap completely between the 11 and 5 mm diameter tubes at high flow rates. A large difference is seen between the larger diameters and the 5 mm diametermonoliths. We have fit two curves, one connecting the 18 mm and 11 mm data and the other connecting the 18 mm data with the 5 mm data for all species. We have reproduced this data on three independently prepared monoliths, and the data collected over all the monoliths is similar indicating a fundamental difference between the 11 and 5 mm diameter tubes as will be discussed later.

As the space velocity increases, the selectivity to CO decreases and the selectivity to CO_2 increases. Over both the 11 and 5 mm diameter catalyst the change is rather dramatic. The changes in carbon atom selectivity seem to be delayed in the 5 mm monolith relative to the 11 mm monolith. This is seen in panels (a), (b) and (c).

The selectivity to H_2O also increases strongly at high space velocity. The O_2 conversion is complete up to 4.4×10^5 h^{-1}, but beyond this space velocity the O_2 conversion decreases rapidly. The conversion of CH_4 increases slightly as the space velocity increases from 5×10^4 to 1×10^5 h^{-1} but decreases steadily beyond that point. The peak in CH_4 conversion corresponds directly with a peak in H_2 selectivity.

The exit temperature of the monolith for CH_4 oxidation increases by 600°C as the space velocity increases from 6×10^4 to 4×10^6 h^{-1}; however, the inlet temperature steadily decreases from 1000°C at 6×10^4 to 70°C at 1×10^6 h^{-1}. When the space velocity is increased to 1.7×10^6 h^{-1}, inlet temperature *apparently* rises to 800°C then steadily falls to about 300°C at 4×10^6 h^{-1}. In all cases the measured exit temperature was within 100°C of the calculated adiabatic temperature.

5. METHANE COUPLING

At low (6×10^4 h^{-1}) and very high (4×10^6 h^{-1}) space velocities the products consists of only CO, CO_2, H_2O, H_2 and unreacted gases, with <0.1% of other products. However, at intermediate space velocities, a significant amount of methane coupling products are observed. This is surprising because previous studies have reported little or no methane coupling products in similar reactor configurations (4, 6). Figure 3 shows the carbon atom selectivity to C_2H_6 and C_2H_4 as a function of space velocity. As the space velocity increases from 1×10^5 h^{-1} the selectivity to C_2H_4 increases to a maximum of 4.5% at 5.2×10^5 h^{-1} and then decreases to <0.1% at space velocities greater than 8×10^5 h^{-1}.

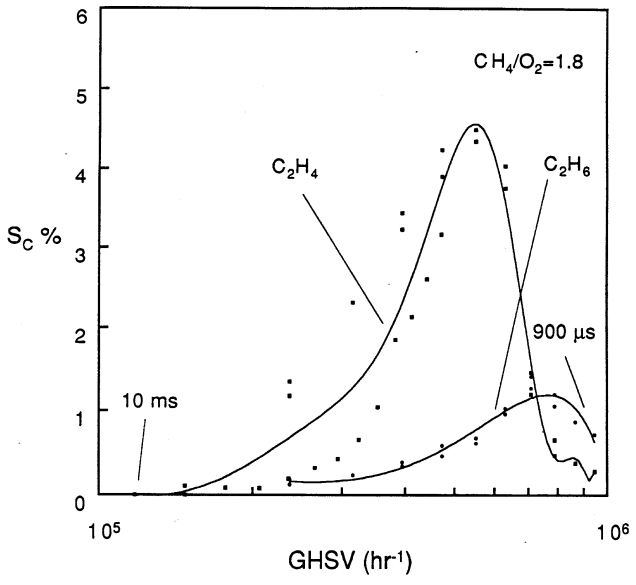

FIG. 3. Methane coupling products. Carbon atom selectivity to methane coupling products. Space velocities are calculated at standard temperature and pressure. $CH_4/O_2 = 1.8$, 20% N_2.

Oxygen variation. Intuitively, as the CH_4/O_2 ratio increases the selectivity to methane coupling reactions should increase because dimerization of CH_3 becomes favored over oxidation reactions. Figure 4(a) and (b) show the carbon atom selectivity, (c) shows the hydrogen atom selectivity and (d) shows the oxygen and CH_4 conversion as a function of fuel to oxygen ratio at a constant space velocity of 4.4×10^5 h^{-1}.

At $CH_4/O_2 = 2.6$, only a fraction of a percent of methane coupling products are detected. However, as the concentration of O_2 in the feed increases, the selectivity to coupling products increases to 9% at $CH_4/O_2 = 1.4$. As the O_2 concentration increases, maxima in different coupling products are observed: C_2H_6 reaches a maximum at $CH_4/O_2 = 2.0$, C_2H_4 at 1.6 and C_2H_2 near 1.4. Ratios below 1.4 were not attempted due to the extremely high temperatures (Fig. 4(e)) and concern with metal evaporation.

The conversion of CH_4 depends strongly on the concentration of O_2, dropping to 70% when the O_2 concentration was cut in half. The O_2 conversion also decreases from 100% at $CH_4/O_2 = 1.4$ to 66% at $CH_4/O_2 = 2.6$. Since the conversion of a particular reactant is independent of initial concentration for first order kinetics, Fig. 4(d) gives evidence that the primary reaction may not be first order in O_2. However, this data could also be interpreted as an indication of variation in mass transfer limitations within the reaction zone.

The temperature of the front and back faces of the monolith are shown in Fig. 4(e). The exit temperature decreases from 1600°C at $CH_4/O_2 = 1.4$ to 1200°C at $CH_4/O_2 = 2.1$, while the entrance temperature decreases only ~50°C from

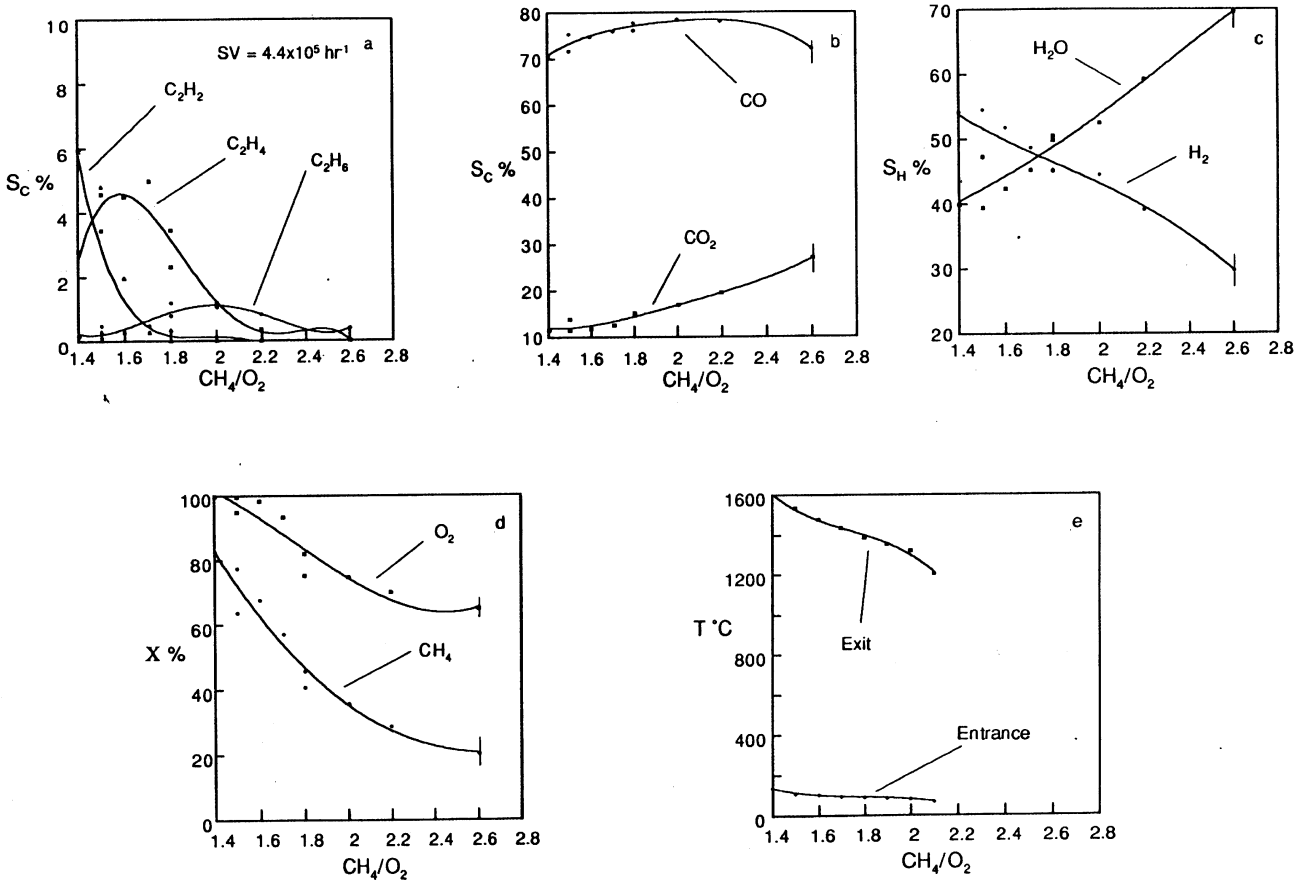

FIG. 4. Methane coupling. Carbon atom (a), (b) and hydrogen atom (c) selectivities, conversion of CH_4 and O_2, and temperatures (e) for the partial oxidation of methane. The vertical lines indicate limits of operation. SV = 4.4×10^5 h^{-1}, 20% N_2, 11 mm diameter Rh supported monolith.

140°C. The increase in exit temperature is a direct result of the increase in conversion.

Dilution. Mass transfer limitations were investigated by varying dilution with N_2. Since the reactor was nearly adiabatic, varying the level of dilution should strongly affect the reactor temperature. The effects of dilution are shown in Fig. 5. Panels (a) and (b) show the carbon atom selectivity, (c) shows the hydrogen atom selectivity, (d) shows the entrance and exit temperature of the monolith and panel (e) shows the O_2 and CH_4 conversion as a function of N_2 dilution at a constant space velocity of 4.4×10^5 h^{-1}. Dilution below 5% was not examined because N_2 was used for GC calibration. Increasing the dilution above 45% resulted in reaction extinction for these conditions.

As the feed stream was diluted at constant space velocity, the methane coupling products disappear. Similar to the space velocity and O_2 concentration experiments, the methane coupling products show a sequential pattern with increasing dilution. At 5% dilution, C_2H_2 is the dominant coupling product (5.5%); however, as the level of dilution increases to 25%, C_2H_4 becomes dominant (5%). As the dilution increases further, C_2H_6 becomes the preferred product, although only 1% selective. In all of these experiments we found no evidence of carbon, which would be a C_2H_2 decomposition product.

In contrast, the selectivity to CO (~70%) remains constant over the entire range of dilution. The independence of the CO selectivity from dilution indicates that CO may only be produced on the catalytic surface. The selectivity to CO_2 also remains constant from 5% to 25% dilution, and as the feed stream is diluted further, the CO_2 selectivity begins to rise. The increase in CO_2 selectivity seems to correspond with the start of incomplete O_2 conversion (e). Therefore, the excess O_2 may react with CH_4, CO, or any methane coupling product to produce an increase in CO_2.

The exit and entrance temperatures decrease by only 100° as the dilution increases from 5% to 40%. This could be the result of a small decrease in conversion; however, the CH_4 conversion drops (e) from 80% to 40%. The catalyst temperature remains relatively constant because of the switch from partial oxidation products to complete oxidation products.

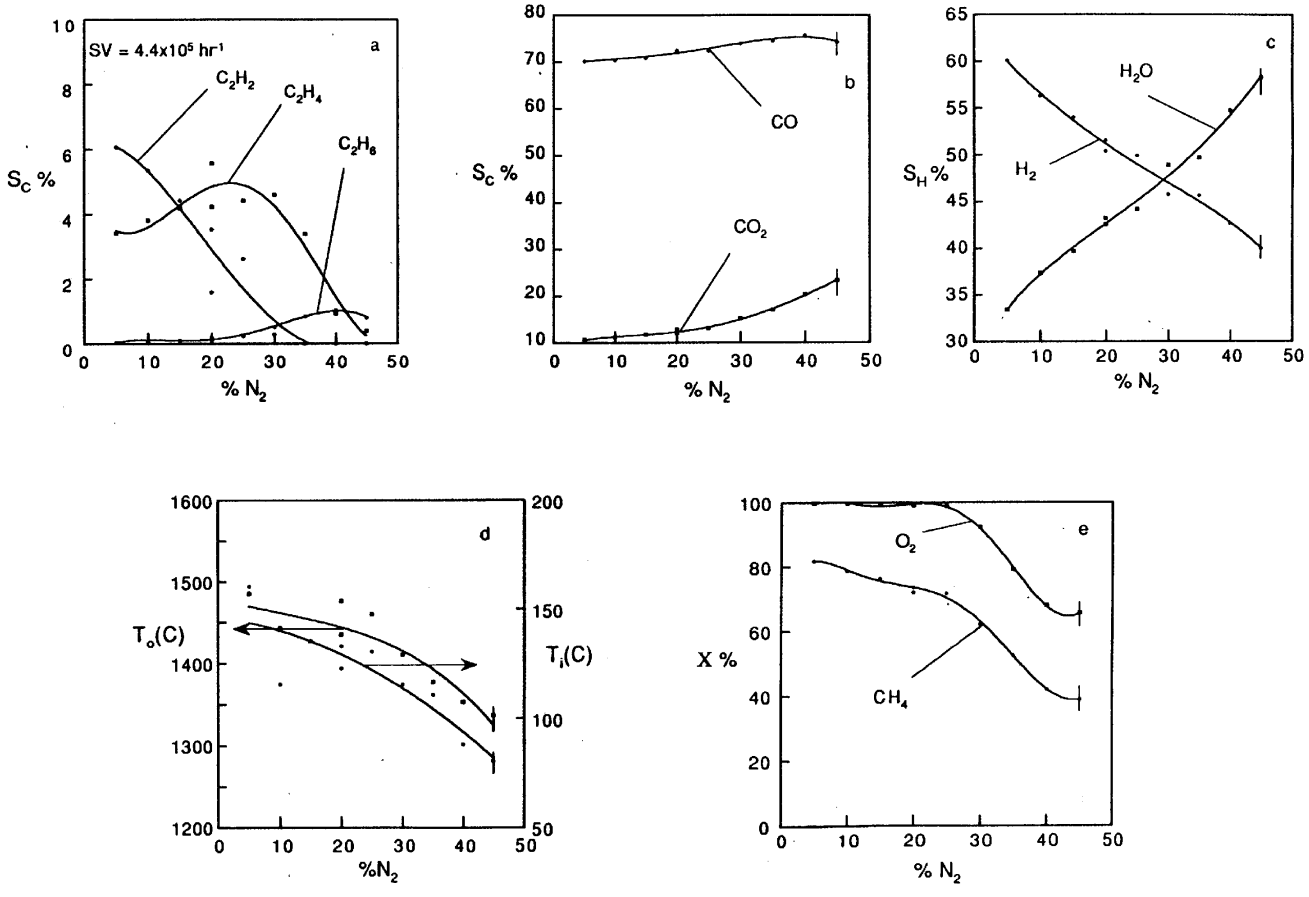

FIG. 5. Methane coupling. Carbon atom (a), (b) and hydrogen atom (c) selectivities, reactor temperatures (d) and the conversion of CH_4 and O_2 (e) for the partial oxidation of methane. SV $= 4.4 \times 10^5$ h^{-1}, $CH_4/O_2 = 1.8$, 11 mm diameter Rh supported monolith.

Preheat. At sufficiently high space velocity, the conversion of O_2 and CH_4 is incomplete. In an attempt to improve reactant conversion at high space velocities, the feed stream was preheated. Figure 6 shows the effect of preheating the gases by 270°C. At up to space velocities of 6.2×10^5 h^{-1} the O_2 conversion increases from 60% to 90% and the CH_4 conversion increased from 35% to 55% when the preheat temperature is 270°C.

When the reactants were preheated, the selectivity to all methane coupling products increase and their maxima move to higher space velocities. The most dramatic increase is in the selectivity to C_2H_4 which increasedfrom 4.5% at 4.5×10^5 h^{-1} to 7.5% at 6×10^5 h^{-1}. The increase in temperature appears to promote methane coupling and the dehydrogenation of C_2H_6 to C_2H_4.

Preheat has little effect on the selectivity to CO and CO_2, and only a slight decrease in the CO_2 production (Fig. 6(e)) and only at the highest space velocities studied. At higher preheat levels, the selectivity to H_2O decreases by about 10%, while the selectivity to H_2 increases by nearly the same amount. It is interesting to note that the differences are only seen at space velocities above 4×10^5 h^{-1}, where the O_2 conversion begins to decrease.

6. DISCUSSION

Ethylene from Ethane

One striking result from these experiments is the extremely large amount of material that can be processed by small amounts of catalyst, >100 tons/day for a 1 foot diameter monolith using ~6 grams of Pt. For space velocities up to 4×10^6 h^{-1} and contact times down to 200 μs, essentially no change in product selectivities and C_2H_6 conversion is observed. Thus, the conversions and selectivities are nearly independent of SV, τ, and v_0 over a factor of at least 50 in flow rate. Increasing the space velocity beyond 3×10^6 h^{-1}, results in a slight loss of C_2H_6 conversion, causing a small drop in C_2H_4 yield.

It might be expected that C_2H_4 is limited by its decomposition in a series process,

$$C_2H_6 \rightarrow C_2H_4 \rightarrow CO.$$

The insensitivity of C_2H_4 and CO to residence time clearly argues against this mechanism, and suggests that C_2H_4 and CO are produced by parallel reactions.

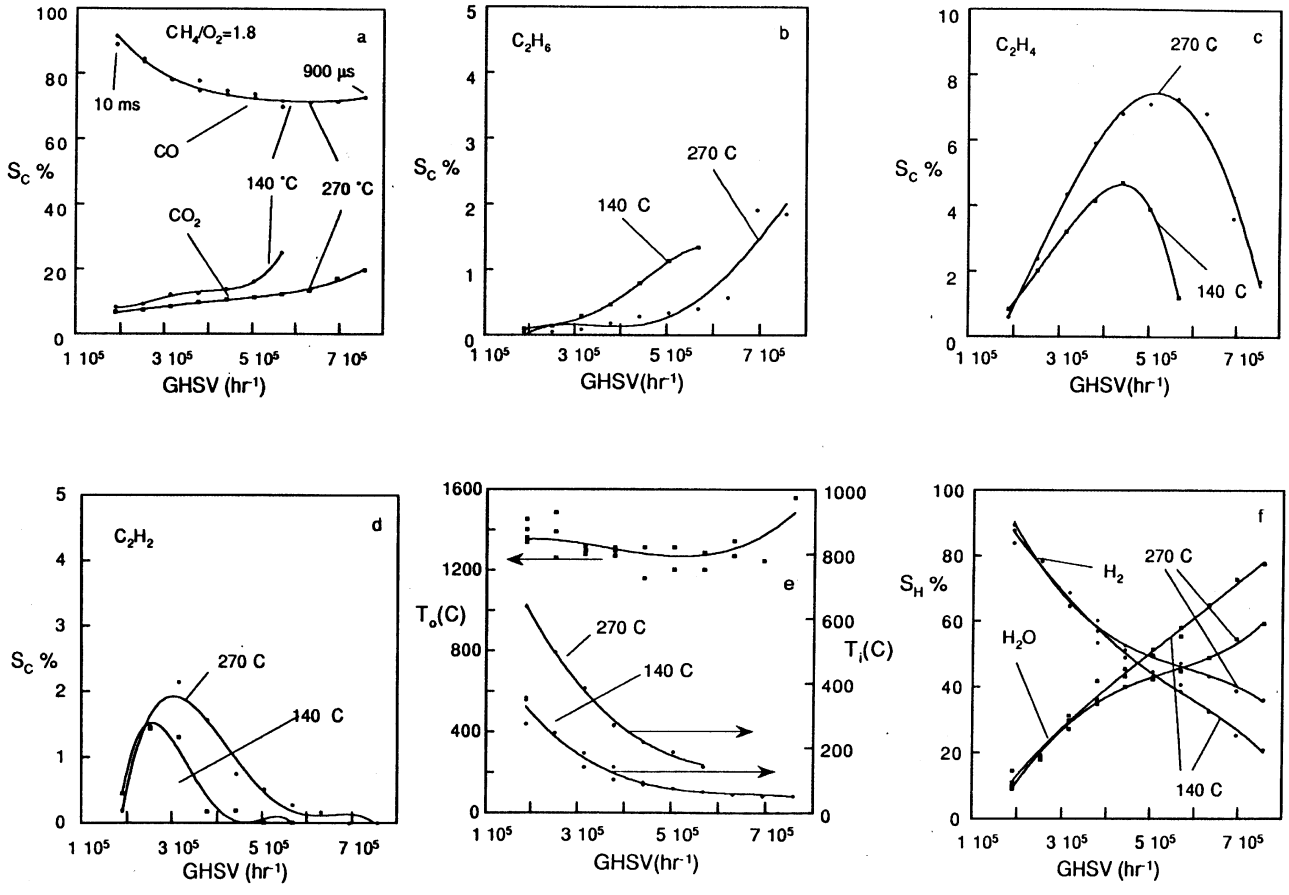

FIG. 6. Methane coupling. Carbon atom (a), (b), (c), (d) and hydrogen atom (f) selectivities and reactor temperature (e) for the partial oxidation of methane. $CH_4/O_2 = 1.8$, 20% N_2, 11 mm diameter Rh supported monolith. Space velocities are calculated at standard temperature and pressure.

Syngas from Methane

One reason the selectivities remain high for C_2H_6 partial oxidation at 1.2×10^6 h^{-1} is that O_2 conversion remains complete. Over the 50-fold increase in space velocity, only small decreases in CO and H_2 selectivities and small increases in H_2O and CO_2 selectivities are detected. This is very different than CH_4 where O_2 breakthrough occurs and product selectivities begin to shift toward combustion products at higher space velocity.

Figure 3 shows that the conversion of CH_4 drops continually as the space velocity increases, while the conversion of C_2H_6 remains high at 85% over the entire range of space velocities. This difference is probably related to the relative sticking coefficients of C_2H_6 on Pt and CH_4 on Rh. The rate of adsorption of CH_4 on Rh films at low temperatures has been studied previously by Brass and Ehrlich (34) who reported a pre-exponential of 3×10^4 $Torr^{-1}$ s^{-1} and an activation energy of 5 to 7 kcal/mol, which corresponds to a sticking coefficient of ~0.01 at 900°C. We have shown that for C_2H_6, the contact time required for reaction is at least a factor of 5 smaller than for CH_4. This implies that the sticking coefficient of C_2H_6 on Pt is at least 5 times the sticking coefficient of CH_4 on Rh at these temperatures. The rate of adsorption of C_2H_6 on Pt has been measured to be 8.8×10^3 $Torr^{-1}$ s^{-1} with no activation barrier (35). This corresponds to a sticking coefficient of ~0.05; which is 5 times the sticking coefficient of CH_4 on Rh. This suggests that the processes are always limited by sticking coefficients at high flow rates.

Mechanism

Syngas formation has been suggested to proceed by three routes: (1) homogeneous reaction of surface generated radicals, (2) heterogeneous combustion followed by steam reforming and water gas shift, and (3) heterogeneous direct oxidation to synthesis gas. These three routes will be examined in relation to the data presented here.

An important aspect in interpreting these results is the variation in temperature profiles within the catalyst as the flow rate is varied as sketched in Fig. 7(a). Previous researchers have measured a sharp temperature peak at the front of the catalyst bed followed by a region where the

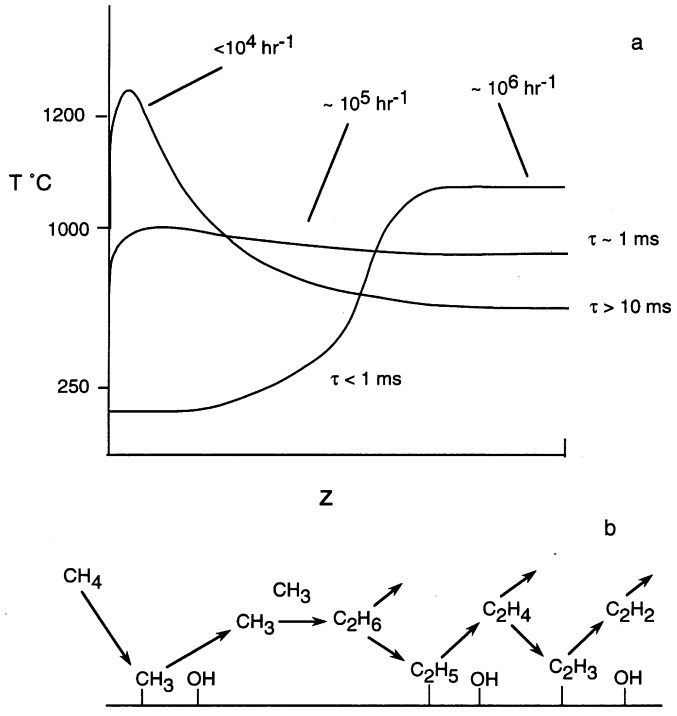

FIG. 7. Schematic temperature profiles within the catalytic monolith for the partial oxidation of methane (a). Schematic mechanism for methane coupling followed by dehydrogenation over Rh supported monoliths (b).

catalyst cools (16, 18). This indicates initial combustion followed by steam reforming occurs at low space velocities. As the space velocity increases to $\sim 10^5$ h^{-1}, the temperature profile becomes more uniform (6), and at very high space velocities the back region of the catalyst becomes hotter than the front region. This suggests that at different space velocities, different routes to syngas and coupling products can occur.

Homogeneous reaction. The catalytic surface may produce free radicals which desorb into the gas phase and further react to form CO, H_2, and other products. A simplified homogeneous reaction scheme has been proposed by Warnatz (12) where two major routes to CO were discussed. One route includes methane coupling intermediates, while the other forms formaldehyde as an intermediate.

Experimentally, we do not detect formaldehyde over the range of space velocities examined, and below 4.5×10^5 h^{-1} little methane coupling products are seen. These experimental facts lead us to believe that a purely homogeneous route to synthesis gas is unlikely. Other researchers have shown that CO can be produced via peroxy radical chemistry (13) although peroxy radical chemistry is only important below 500°C (14), approximately 500°C cooler than our reaction system. Research on CH_4/O_2 mixtures passing a heated foil have shown that the homogeneous ignition temperature above a Rh foil is well above the temperatures, measured at the exit of the catalytic monolith (33).

It has also been shown that the catalyst surface plays a crucial role in determining reaction products. When Pt is substituted for Rh, the selectivity to CO and H_2 decrease strongly due to differences between the activation energies for the formation of OH on the metal surface (6). Gas phase radicals are stabilized and thus quenched when they absorb on a metallic surface. This is especially true for low molecular weight radicals like CH_3. Because of this stabilization, the surface probably acts as a radical sink, rather than a radical source. Also, at reaction times less than 10^{-3} sec, sufficient time is not available for radicals to build up in the gas phase. Therefore, we feel that surface promoted gas-phase reactions are not occurring at substantial levels.

Indirect formation of syngas. Many investigators have examined the conversion of CH_4 to syngas over different catalysts (15–23), and several have suggested that a small amount of CH_4 combusts initially,

$$CH_4 + 2O_2 \rightarrow CO_2 + 2H_2O, \qquad [8]$$

and the heat liberated by combustion then drives the endothermic steam [2] and CO_2 reforming reactions,

$$CH_4 + CO_2 \rightarrow 2CO + 2H_2. \qquad [9]$$

As a secondary process the products may further react via the water-gas-shift reaction [3]. These reactions should lead to a sharp temperature spike near the front part of the catalyst bed because of the greater exothermicity of total combustion, and H_2O and CO_2 have been measured in short beds in some reactor systems (15, 16, 18, 24). However, most of the previous work has used space velocities below 6×10^4 h^{-1}.

The experimental measurement of a temperature spike gives strong evidence for complete combustion followed by reforming and shift reactions. At low space velocities (below 1×10^5 h^{-1} we feel this may be occurring because the contact time is large enough to allow for complete combustion and for the relatively slow reforming reactions to follow. The presence of H_2O and CO_2 at short times appears to suggest this process. We argue below why this is not the case at space velocities greater than 10^5 h^{-1}.

Direct formation of synthesis gas. Our work has focused on space velocities above 1×10^5 h^{-1}, which corresponds to a contact time $\leq$10 ms. We have shown that at contact times near 1×10^5 h^{-1}, the partial oxidation of CH_4 to CO and H_2 is >90% selective at ~90% conversion (2, 6). The temperature profile along the axis of the catalytic monolith was found to be nearly flat (6). As the space velocity increases beyond 1×10^5 h^{-1}, the temperature profile begins to change. The front of the catalyst cools while the exit temperature increases by up to 200°. Figure 7(a) shows

qualitatively the temperature profiles within the catalytic monolith at different space velocities.

At space velocities below $1 \times 10^5\ h^{-1}$, the maximum temperature is greater than the exit temperature. This temperature spike may be caused by complete combustion followed by a temperature decrease due to the endothermic reforming reactions as reported elsewhere (15–23). At these space velocities the contact time is sufficiently large to allow these reactions to occur. However, as the space velocity approaches $1 \times 10^5\ h^{-1}$, the contact time has decreased to a point where the reforming and combustion reactions are no longer occurring. At $1 \times 10^5\ h^{-1}$, the contact time is sufficient to support the direct partial oxidation of CH_4 to syngas [1].

As the space velocity increases significantly beyond $1 \times 10^5\ h^{-1}$, the temperature of the front region of the catalytic monolith decreases substantially. At these temperatures, the formation of combustion products is favored over partial oxidation products. We believe that the cool region of the monolith is producing the CO_2 and H_2O. Therefore, as the temperature of the leading edge is driven down by an increase in space velocity, the selectivity to CO_2 and H_2O should increase, as observed.

If the cool portion of the monolith plays an important role in the formation of CO_2 and H_2O, then preheating the feed gases should reduce the amount of complete combustion products detected. Figure 6 shows that as preheat is added to the system, the selectivity to H_2O and CO_2 decrease in agreement with the mechanism. Also Fig. 5 shows that as N_2 is removed from the feed stream, the selectivity to complete combustion products decreases. Both of the these experiments point to the importance of the cool leading edge in the production of CO_2 and H_2O.

Methane Coupling

Methane coupling has been extensively studied in many different configurations and for many different catalysts (25–31). Below 800°C the production of C_2's from CH_4 is believed to follow a surface initiated homogeneous reaction pathway, as sketched in Fig. 7(b). CH_4 absorbs dissociatively on an oxygen covered surface forming CH_3 and OH. It appears that at sufficient space velocities the CH_3 radical desorption rate is faster than the rate of complete pyrolysis of CH_4 to C and H. This CH_3 desorbs and combines in the gas phase with a second CH_3 to form C_2H_6. At high space velocities the temperature of the front part of the monolith is below 800°C (Fig. 7(a)), and these temperatures appear to allow formation and desorption of CH_3, while at higher temperatures CH_4 decomposes completely to C's.

It is unclear at this point whether the CH_3 radicals are formed on the Rh or the alumina surfaces. We are presently investigating the effect of low loadings of metal and different ceramic supports to determine the catalytic activity of metal and oxide at these reaction conditions.

These results suggest that the cool portion of the monolith promotes the formation and desorption of CH_3 radicals and that C_2H_6 is formed prior to reaching the hot zone near the exit of the catalyst. As sketched in Fig. 7(b), the C_2H_6 may adsorb on the Rh surface and dehydrogenate to form C_2H_4. At high reaction temperatures the C_2H_4 may further dehydrogenate to form C_2H_2 as shown by the dilution and preheat experiments. The experimental results give strong evidence for a series reaction scheme from C_2H_6 to C_2H_4 and on to C_2H_2 because of the observed relation with flow rate, dilution, and composition in these products.

The results also show a strong decrease in the production of methane coupling productions beyond $4.5 \times 10^5\ h^{-1}$. This coincides exactly with the onset of significant oxygen breakthrough. We believe that the excess O_2 combusts the highly reactive C_2 products (primarily to CO_2). This explains the loss in C_2 selectivity and the support of the O_2 conversion as the space velocity increases beyond $4.5 \times 10^5\ h^{-1}$. The significance of O_2 breakthrough on the decrease in C_2 selectivity is seen in the CH_4/O_2 ratio, dilution, and preheat experiments. At a CH_4/O_2 of about 1.8, the onset of significant O_2 breakthrough occurs. This coincides with a strong decrease in the total selectivity to coupling products. When the dilution was increased beyond 25%, oxygen breakthrough occurs and coupling products begin to disappear. Finally, when the feed is preheated, the onset of O_2 breakthrough is delayed. This delays the decrease in selectivity to coupling products by exactly the same amount.

Effect of Reactor Tube Diameter

Figures 1 and 2 show data from 3 different reactor tube diameters: 18 mm, 11 mm, and 5 mm. In each case the length of the monolith and radiation shield remained constant. The data collected from the 18 and 11 mm diameter tubes were reproducible and connect quite well. However, the data from the 5 mm monolith differs slightly for the C_2H_6 system but differs significantly for CH_4 from the trends set by the 18 and 11 mm data. We reproduced this on several independently prepared monolith samples, although we have not been able to confirm the cause of the difference.

Three different factors may be altering the results. (1) As the space velocity increases, the monoliths should operate closer to adiabatic. This would promote a flatter temperature profile across the catalyst, which in turn would improve the selectivity and conversion as shown by data within this report. (2) The flow pattern entering the catalyst may have an effect on product distribution. The calculated Reynolds number for the feed gases in the tube prior to entering the catalyst is approximately 1000 for 18 mm, 1500 for 11 mm, and 2700 for 5 mm. This suggests that the fluid entering the catalyst was laminar for the 18 and 11 mm diameter tubes; however, the flow may be turbulent in the 5 mm tube. The turbulent flow would create a more uniform concentration profile across the catalyst, promoting better reaction and

therefore higher conversions and selectivities. (3) The catalyst geometry may also have a significant effect on product distribution. The pore diameter of a 45 ppi monolith is approximately 0.5 mm, which corresponds to a characteristic pore to monolith diameter ratio of 0.1 for a 5, 0.05 for an 11, and 0.03 for an 18 mm monolith. The difference in this ratio could cause a significant effect on the flow patterns through the monolith, causing the increase in selectivities and conversions.

The data collected from the 5 mm monolith at $SV > 4 \times 10^6\ h^{-1}$ and $\tau \sim 200\ \mu s$ indicates that these reaction systems could perhaps be significantly improved. As the space velocities were increased, the ensuing turbulence or improved adiabatic operation may improve the product selectivities and CH_4 conversion. This is a significant factor in designing an efficiently operating syngas reactor, and more experiments to elucidate the apparent effects of reactor diameter would require studies on pilot plant scale to determine the limiting residence time in syngas production.

7. CONCLUSIONS

We find that ethylene can be produced from C_2H_6 at space velocities as high as $4 \times 10^6\ h^{-1}$ ($\sim 200\ \mu s$) over Pt coated monoliths without much loss in selectivities or conversion. In contrast, CH_4 conversion decreases steadily with an increase in space velocity above $10^5\ h^{-1}$.

We believe that these experiments support the direct oxidation of CH_4 to synthesis gas at high space velocities even though CO_2 and H_2O increase. The loss in selectivity to synthesis gas at high space velocities can be attributed to the cool front region of the catalyst which favors the formation of complete combustion products and also the formation of CH_3 radicals which lead to C_2 products. We find at the proper space velocity, preheat, and dilution the selectivity to methane coupling products can be enhanced over Rh coated foam monoliths. We also find strong evidence that C_2H_4 and C_2H_2 is formed via series reactions from C_2H_6. At high space velocities the selectivity to C_2 products, decreases due to O_2 breakthrough and homogeneously combusting with the highly reactive coupling products. Further experiments on coupling reactions in different metal and catalyst geometries are in progress.

REFERENCES

1. Hickman, D. A., and Schmidt, L. D., *J. Catal.* **138**, 267 (1992).
2. Torniainen, P. M., C., X., and Schmidt, L. D., *J. Catal.* **146**, 1 (1994).
3. Bharadwaj, S. S., and Schmidt, L. D., *Fuel Process. Technol.* **42**, 109 (1995).
4. Bharadwaj, S. S., and Schmidt, L. D., *J. Catal.* **146**, 11 (1994).
5. Hickman, D. A., and Schmidt, L. D., *AIChE J.* **39**, 1164 (1993).
6. Hickman, D. A., and Schmidt, L. D., *Science* **259**, 343 (1993).
7. Huff, M., and Schmidt, L. D., *J. Phys. Chem.* **97**, 11815 (1993).
8. Hickman, D. A., Haupfear, E. A., and Schmidt, L. D., *Catal. Lett.* **17**, 223 (1993).
9. Hickman, D. A., and Schmidt, L. D., *J. Catal.* **136**, 300 (1992).
10. Huff, M., and Schmidt, L. D., *J. Catal.* **149**, 127 (1994).
11. Huff, M., and Schmidt, L. D., *J. Catal.* **155**, 82 (1995).
12. Warnatz, J., "Chemistry of High Temperature Combustion of Alkanes up to Octane." Twentieth Symposium (International) on Combustion, The Combustion Institute, pp. 845–856, 1984.
13. Ranzi, E., *et al., Combust. Sci. Technol.* **96**, 279 (1994).
14. Lewis, B., and Elbe, G. V., "Combustion, Flames and Explosions of Gas," 3rd ed., Academic Press, London, 1987.
15. Dissanayake, D., Rosynek, M. P., Kharas, K. C. C., and Lunsford, J. H., *Journal of Catalysis* **132**, 117–127 (1991).
16. Prettre, M., Eichner, C., and Perrin, M., *Trans. Faraday Soc.* **43**, 335 (1946).
17. Mouaddib, N., *et al., Appl. Catal. A* **87**, 129 (1992).
18. Dissanayake, D., Rosynek, M. P., and Lunsford, J. H., *J. Phys. Chem.* **97**, 3644 (1993).
19. Choudhary, V. R., Rajput, A. M., and Prabhakar, B., *J. Catal.* **139**, 326 (1993).
20. Bhattacharya, A. K., *et al., Appl. Catal. A* **80**, L1 (1992).
21. Ashcroft, A. T., *et al., Nature* **344**, 319 (1990).
22. Ashcroft, A. T., *et al., Nature* **352**, 225 (1991).
23. Vernon, P. D. F., *et al., Catal. Lett.* **6**, 181 (1990).
24. Hochmuth, J. K., *Appl. Catal. B: Environ.* **1**, 89–100 (1992).
25. Lin, P. Z., *et al., Appl. Catal. A* **131**, 207 (1995).
26. Mariscal, R., Pena, M. A., and Fierro, J. L. G., *Appl. Catal.* **131**, 243–261 (1995).
27. Bajus, M., and Back, M. H., *Appl. Catal.* **128**, 61 (1995).
28. Wang, W., and Lin, Y. S., *J. Membrane Sci.* **103**, 219 (1995).
29. Wang, D., Rosynek, M. P., and Lunsford, J. H., *J. Catal.* **155**, 390 (1995).
30. Nibbelke, R. H., Scheerová, J., de Croon, M. H. J. M., and Marin, G. B., *J. Catal.* **156**, 106 (1995).
31. Bjorklund, M. C., and Carr, R. W., *Catal. Today* **25**, 159 (1995).
32. Huff, M., and Schmidt, L. D., submitted for publication.
33. Ziauddin, M.E., and Schmidt, L. D., to be published.
34. Brass, S. G., and Ehrlich, G., *J. Chem. Phys.* **87**(8), 4285 (1987).
35. Carter, E. A., and Koel, B. E., *Surf. Sci.* **226**, 339 (1990).
36. Hultgren, R. *et al.*, "Selected Values of the Thermodynamic Properties of the Elements," Amer. Soc. Metals, Metals Park, Ohio, 1973.